Materials International
Open Access Journal (ISSN: 2668-5728)

Article
Volume 6, Issue 3, 2024, 26
https://doi.org/10.33263/Materials63.026

Synthesis, Crystal Structure, Optical, Electrochemical Investigations of La_2ZrZnO_6 Ceramic Nanoparticles

Madhukumar H. N. [1], Shivakumar P. [1,*], Manoj M. [1], Ramesh S. [1], Yogesh T. G. [1]

[1] School of Physical Sciences, Amrita Vishwa Vidyapeetham, Mysuru Campus, Mysuru – 570 026, Karnataka, India
* Correspondence: shivumodi973@gmail.com;

Scopus Author ID N.A.
Received: 1.07.2024; Accepted: 1.09.2024; Published: 10.09.2024

Abstract: Herein, we describe the synthesis and characterization of La_2ZrZnO_6 (LZZO) nanoparticles using the sol-gel method. The structure and morphology of as-prepared nanoparticles were characterized using powder X-ray diffraction (PXRD), scanning electron microscopy (SEM), UV-visible spectroscopy, and impedance spectral analyses. The XRD pattern reveals that the average crystallite size of the as-prepared LZZO nanoparticles is 169 nm. The as-prepared nanoparticles show an orthorhombic crystal perovskite system with two distinct types of small and large pores distributed uniformly across the surface area. On the other hand, the Ramna spectral investigations revealed the stretching and bending vibrations within the as-prepared nanomaterial. Furthermore, AC electrical studies and impedance analysis of LZZO nanoparticles were examined using dielectric studies. As-prepared LZZO nanoparticles exhibited a superior dielectric function, thus indicating its potential for use in energy harvesting applications. The photocatalytic degradation studies of LZZO nanoparticles against methylene blue (MB) dye were assessed under light, demonstrating the potential property exposure to determine its photocatalytic activity.

Keywords: La_2ZrZnO_6 nanoparticles; PXRD; DRS; dielectric studies.

1. Introduction

The escalating energy demands coupled with rapid climate changes have spurred scientists to devise eco-friendly solutions for clean energy applications [1, 2]. Various approaches have been proposed to develop multifunctional materials capable of exhibiting optical, electrical, and electrochemical properties [3]. This trend stems from the demand to curtail power consumption while enhancing the functionality of next-generation electronic devices [4]. Semiconductor materials that catalyze chemical reactions to light exposure hold significant promisefor environmental remediation, including water and air purification and energy conversionapplications such as solar cells and hydrogen production [5].

Perovskite materials, renowned for their magnetic, electronic, and structural properties, have gained widespread attention. Single perovskites, denoted by ABO_3, are filled with alkali or rare earth metals in the A-site and transition metals in the B-site [6, 7]. Perovskite solar cells are emerging as affordable and efficient solutions for solar energy conversion [8]. Their optoelectronic properties make them suitable for LEDs, lasers, and photodetectors. Additionally, perovskite-based catalysts show high activity in various catalytic and photocatalytic reactions, which are essential for energy conversion and environmental applications [9]. Transitioning single perovskite into doubleperovskites ($A_2BB'O_6$) enhances thermal stability, carrier mobility, and safety [3, 10]. Double perovskite solar cells have seen a dramatic increase in efficiency, now exceeding 25%. Double perovskites like Sr_2FeMoO_6 and Ba_2NaOsO_6 exhibit high magnetoresistance and are promising for spintronics with narrower band gaps [11].

Lanthanum oxide (La_2O_3) is appreciated for its high refractive index, making it valuable in opticalmaterials [12]. With their high dielectric constant and excellent thermal stability, Lanthanum oxide nanoparticles find applications in diverse industries because of their unique chemical, catalytic,magnetic, and electronic properties. Zinc oxide (ZnO) is another crucial material in the UV-Vis region used as a sensor [13]. As a wide bandgap semiconductor, zinc oxide is utilized in various optoelectronic devices such as LEDs, photodetectors, and solar cells. The double perovskites with zirconium are rarely available [14]. Its thermal expansion properties benefit refractory materials, while its chemical inertness and ability to conduct oxygen ions at high temperatures make it a preferred electrolyte for SOFCs [15].

We synthesized the Zr-based La2ZrZnO6 double perovskite using the cost-effective sol-gel method in this study. Subsequently, we investigated the synthesized material's optical and electrochemical properties per the literature report [16].

2. Materials and Methods

2.1. Materials and methods.

Lanthanum nitrate (Avra chemicals, India), zirconium nitrate (Kemphasol, USA), and zinc nitrate (Avra, India) are procured from commercial sources. The PXRD measurements were conducted on an X-Pert Pro diffractometer at ambient temperature utilizing a Cu–Kα radiation source, and the results were gathered throughout the 2θ range of 10° to 80°. The absorption studies were performed on a UV-1800 spectrophotometer (Shimadzu, Japan).

2.2. Synthesis of double perovskites.

The double perovskites La_2ZrZnO_6 nanoparticles were synthesized through a simple sol-gel method. Lanthanum nitrate (4.14 g), zirconium nitrate (6.17 g), and zinc nitrate (2.41 g) are dissolved in 50 mL of water and stirred together for 30 mins. To this, 100 mL of 1 M citric acid was added and continuously stirred for 6 h. The resulting solution turned white, which was then stirred continuously at 80°C until it became a sticky gel. Thus, the obtained gel was dried and calcinated at 700°C for 12 h to get a fine, homogenous, dense powder.

3. Results and Discussion

3.1. X-ray diffraction studies.

The identification of the phases and average crystallite sizesof the LZZO nanoparticles were obtained using PXRD investigation [21]. The measurements were conducted at ambient temperature utilizing a Cu–Kα radiation source, and the results were gathered throughout the 2θ range of 10° to 80° [22]. The PXRD was indexed to the orthorhombic crystal perovskite system [10]. The experimentally observed and refined simulated XRD patterns are displayed in Figure 1, and the average size of FWHM is given in Table 1. Most significant peaks from the experimentally observed pattern matchthe simulated pattern [23-25].

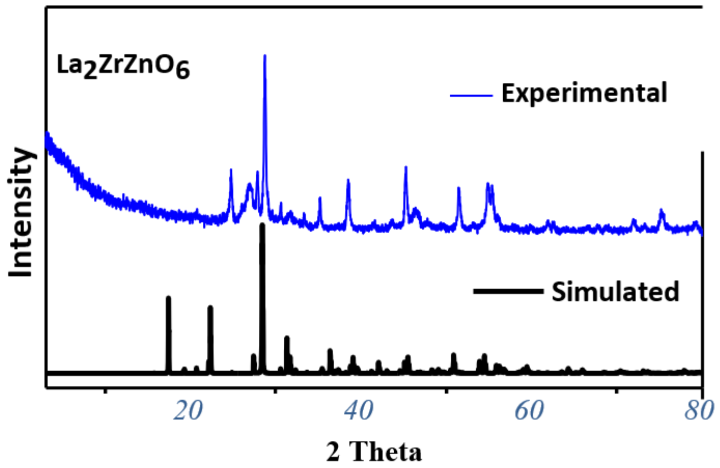

Figure 1. The X-ray diffraction pattern of the LZZO was compared with that simulated pattern.

Table 1. Crystallite sizes of LZZO nanoparticles.

Position [2θ]	FWHM	Size
7.3395	1.2595	66.13
15.9038	0.9446	88.85
22.4880	1.2595	67.29
26.1798	0.4723	180.70
28.5148	0.5510	155.66
30.1062	0.3149	273.35
32.9485	0.4723	183.54
36.3584	0.4723	185.25
44.6132	0.4723	190.25
47.4393	0.6298	144.17
72.2031	0.3936	261.43
73.5408	0.4723	219.75
75.6259	0.5510	191.00

Average Crystallite Sizes = 169.00

3.2. Surface morphology studies.

The sample's surface morphology and quantitative elemental composition were analyzed using scanning electron microscopy (SEM) images and energy-dispersive X-ray spectroscopy (EDS) analysis. Figure 2 represents SEM images showcasing the surface morphology of the LZZO sample at varying magnifications (2 µm, 200 nm, and 100 nm) at different randomly selected locations. The SEM images reveal that the LZZO sample exhibits two distinct types of small and large pores distributed uniformly across the surface area. The presence of large pores can be attributed to the significant release of gas molecules during the heat treatmentprocess. These large pores are homogenously interspersed with smaller pores located within the outer boundaries of the larger one. The morphology observed resembles small island-like structures comprising slightly agglomerated nanoparticles because of the intense heat treatment experienced by the sample. The dispersion of the grain around 150 nm conforms to the material's polycrystalline behavior. The randomly selected particles' EDX profile confirms that the samples are pure and all the constituent elements are present. The elemental quantities analysis (inset Table) confirms that the constituent elements are present in the expected quantities.

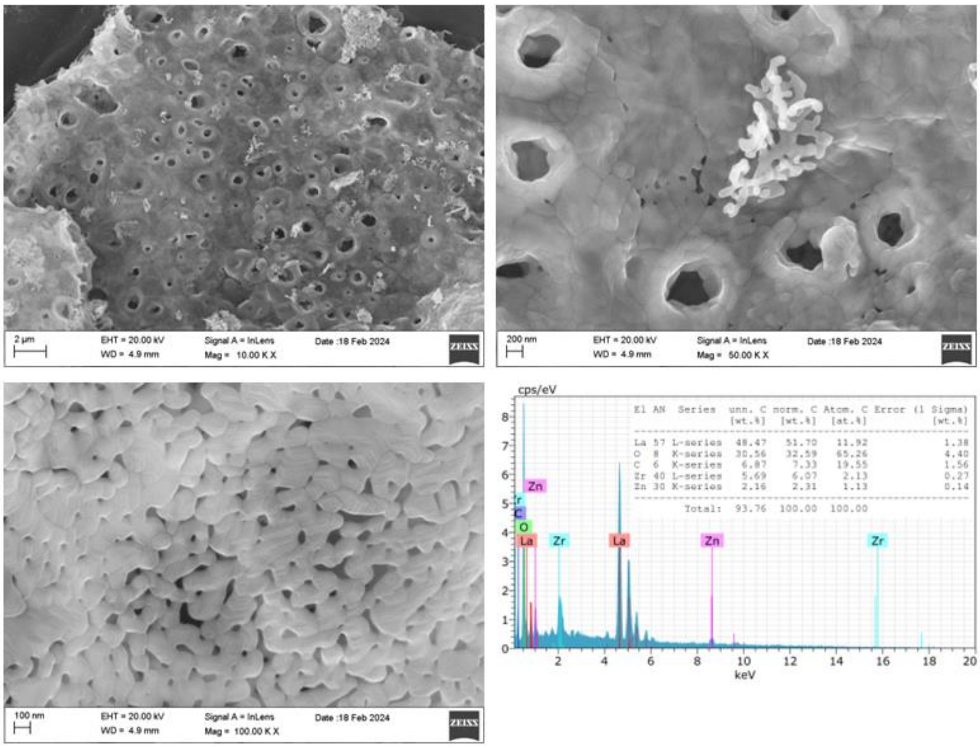

Figure 2. SEM images, EDX- profile, and quantitative analysis (inset Table) of LZZO nanoparticles.

3.3. Raman spectra.

Raman spectra of the as-synthesized LZZO nanoparticles were recorded at room temperature. From Figure 3, it can be seen nine Raman active modes in the range between 80 cm^{-1} to 1090 cm^{-1}. In the lower frequency region, the peaks at 82 cm^{-1} and 106 cm^{-1} are attributed to the bending vibrations of La-O bonds [32]. The peak at 140 cm^{-1} could also be the bending vibrations of La-O and Zn-O bonds [33].

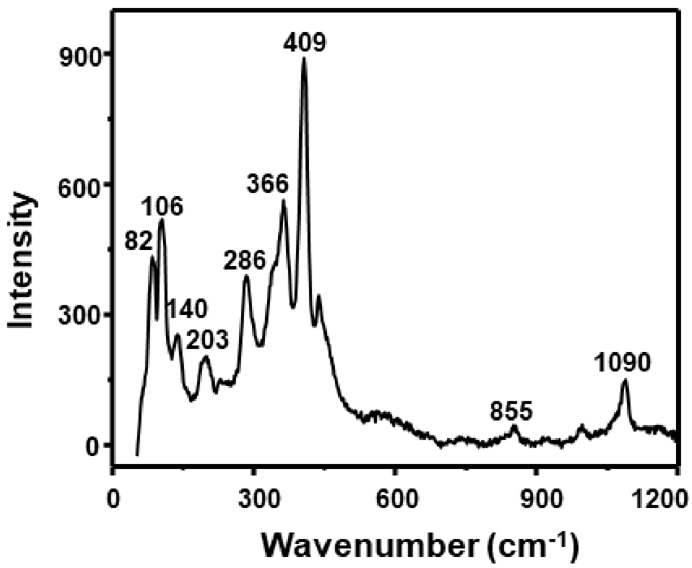

Figure 3. Raman spectrum of the as-synthesized LZZO nanoparticles.

The peak that appeared at 203 cm^{-1} is due to the combination of stretching vibrations of La-O and Zr-O bonds. The peaks at 286 cm^{-1} and 855 cm^{-1} within this range (300-700 cm^{-1}) are attributed to the stretching modes of Zr-O bonds. The peak that appeared at 203 cm^{-1} is due to the combination of stretching vibrationsof La-O and Zr-O bonds. The peaks at 286 cm^{-1} and

855 cm^{-1} are attributed to the stretching modes of Zr-O bonds [34]. The peaks noticed at 366 cm^{-1} and 409 cm^{-1} are ascribed to the pure O-O stretching modes, which are a bit lower than their actual position, which is around 450-550 cm^{-1} appearing positions. These O-O vibrations possibly defects in the LZZO system [34]. This peak is significantly higher than the usual Raman active modes observed in LZZO. It might be due to overtone or combination modes of other vibrations or possibly due to background noiseor contamination in the measurement [34].

3.4. Impedance spectral analysis.

Impedance spectroscopy is a very effective technology used to analyze the electrical properties of materials [34]. Figure 4 displays the frequency-dependent real component of the impedance Z'versus frequency plot at room temperature. The real component of the impedance exhibits distinct behavior depending on the frequency range [35]. At low frequencies until 7.7×10^3, the real part of the impedance decreases rapidly from 6.5×10^6 to 2.5×10^6 as the frequency increases. After that frequency, it gradually decreases. This can be explained by the increase in AC conductivity due to the higher mobility of charge carriers and the decrease in the concentration of trapped charges [36]. At higher frequencies, the Z' curves are almost reduced to reach flat, suggesting the potential release of space charge polarization and subsequent reduction in barrier features inside the material, which increases conductivity [37]. This is inversely proportional to the frequency dependence impedance spectral response, which indicates that the study materials belong to the capacitive materials [38]. At the lower range, the sudden decrease is also associated with the relaxation processes being more accurate at the lower frequencies for this material, as seen by the behavior of the following imaginary component of the impedance Z″.

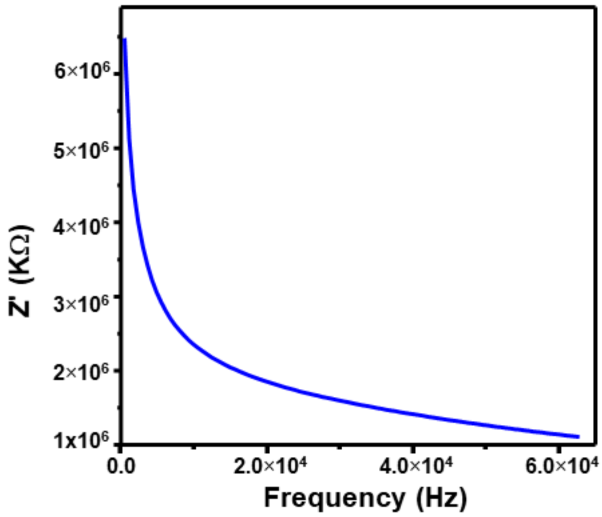

Figure 4. Frequency-dependent dielectric constant of the LZZO nanoparticles.

3.5. optical studies.

Figure 5(a) depicts the UV–Vis–NIR diffuse reflectance spectra (DRS) of LZZO material obtained in the 200–800 nm range. In DRS, a strong band was seen in the 200–800 nm range, with a peak around 450–500 nm. This band relates to the charge transfer band (CTB), which is a band that moves from the O^{2-}ligand to the La^{3+} ions in the host lattice [39]. The optical bandgap energy is generally determined from measured diffuse reflectance spectra, which can be transformed into the corresponding absorption spectra by applying the Tauc plot (equation 1) and Kubelka-Munk equation (equation 2) [41]. Although the K-M plot and the

Tauc plot both evaluate the interaction between light and materials, the K-M plot is superior when it comesto materials that are opaque or scatter light and homogenous samples. Compared to Tauc plots, K-M plots are less susceptible to the effects of scattering and provide a more comprehensive picture since they consider both absorption and scattering effects [42]. Because of this, K-M is a more suitable option for comprehending the entire light interaction in samples of this kind.The optical bandgap of the LZZO can be calculated using the Kubelka-Munk equation.

$$(\alpha h u)^{1/\gamma} = B\ (h\mathrm{P} - Eg) \qquad (1)$$

$$(\mathrm{F}\ (\mathrm{R}) \times h\gamma)^{1/\gamma} = B\ (h\mathrm{P} - Eg) \qquad (2)$$

where h denotes the Planck constant, ν represents the frequency of the photon, Eg signifies the band gap energy, and B is a constant. The γ factor has a different value for the direct and indirect transition band gaps is 1/2 or 2, correspondingly, and is contingent upon the characteristics of theelectron transition. In most cases, the band gap energy is calculated using diffuse reflectance spectra that have been measured and converted to absorption spectra via the Kubelka-Munk equation [43]. The calculated direct and indirect bandgaps of LZZO materials are found to be 2.7eVand 3.2eV, respectively. This optical bandgap value suggests that the LZZO materials could be a potential candidate for photovoltaics and photocatalytic applications [44].

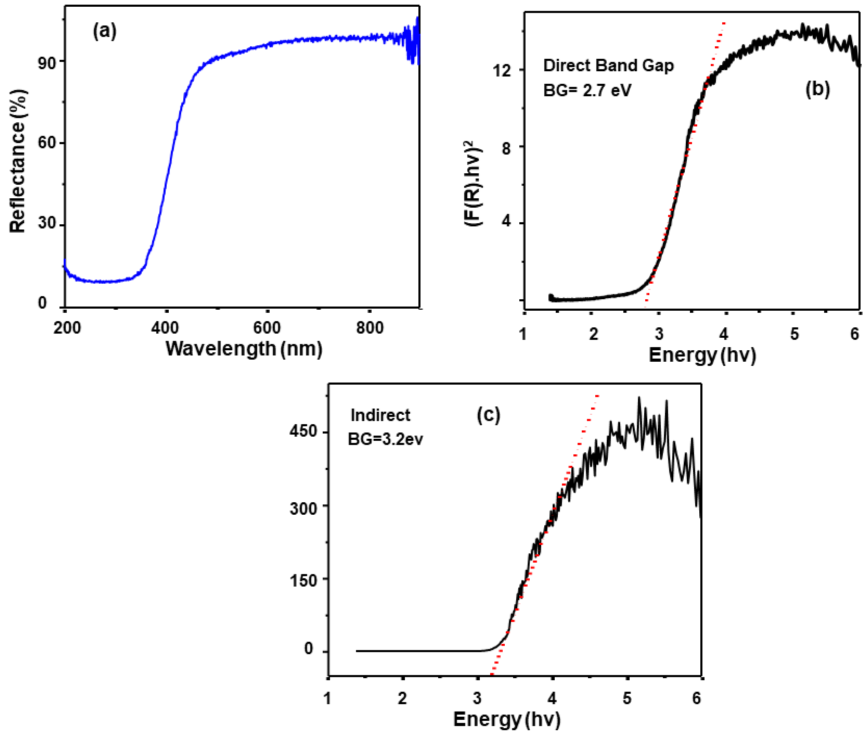

Figure 5. (a) DRS spectrum at room temperature; **(b)** Kubelka-Munk direct bandgap; **(c)** indirect bandgap of the LZZO materials.

3.6. Photocatalysis investigation.

The photocatalytic absorption results of LZZO nanoparticles with methylene blue dye degradation are depicted in Figure 6. The photocatalytic absorption spectra confirm that the maximum absorption of the initial methylene blue dye is gradually degraded over time. The synthesized LZZO sample shows 35% degradation in 60 minutes, revealing that the degradation rate is significantly enhanced as time increases.

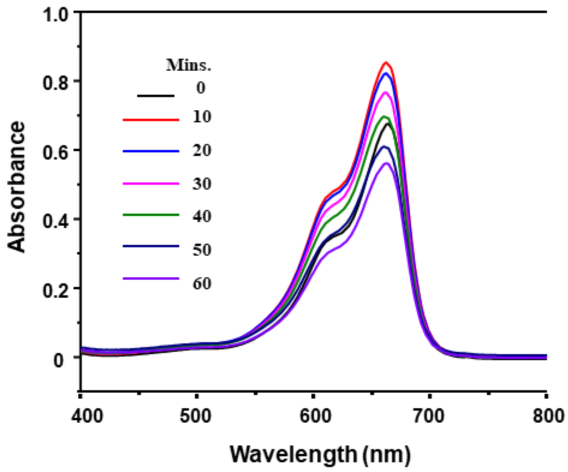

Figure 6. Photocatalytic efficiency of the LZZO nanoparticles.

4. Conclusions

In summary, the extensive examination carried out on LZZO nanoparticles through the utilizationof diverse analytical methodologies has yielded significant observations related to their structural, morphological, electrical, and optical characteristics. The refined crystal structure parameters of the orthorhombic crystal perovskite system, as determined by X-ray diffraction (XRD), indicate a stable configuration. The examination of surface morphology via scanning electron microscopy (SEM) revealed the existence of well-defined nanoparticles and morphology resembling islands, which provided evidence of the synthesis procedure. The LZZO materials' vibrational modes wereadditionally clarified through the utilization of Raman spectroscopy, which provided insights intotheir chemical bonding and possible imperfections. The electrical behavior was revealed by impedance spectroscopy, which revealed conductivity and frequency-dependent impedance characteristics that are crucial for energy storage and electronic device applications. Further, identifying a significant charge transfer band through optical investigations, specifically UV-Vis-NIR diffuse reflectance spectroscopy indicates possible uses in photovoltaics and photocatalysis. In addition to providing further support for these applications, the calculated bandgap energies for direct and indirect bandgaps indicate that the material is suitable for energy conversion and light absorption. Considering these findings, LZZO materials hold promise for various applications. LZZO materials exhibit potential for a multifunctional application, encompassing capacitors, photovoltaic cells, energy storage devices, and photocatalysts for environmental remediation.

Funding

This research received no external funding.

Acknowledgments

Authors extend their appreciation to the Director, Amrita Vishwa Vidyapeetham, Mysuru Campus, for providing instrumentation and infrastructure facilities.

Conflicts of Interest

The authors declare no conflict of interest.

References

1. J.L. Holechek; H.M.E. Geli; M.N. Sawalhah; R. Valdez. A Global Assessment: Can RenewableEnergy Replace Fossil Fuels by 2050. *Sustainability* **2022**, *14*, 4792, https://doi.org/10.3390/su14084792.
2. A. Lavín; R. Sivasamy; E. Mosquera; M.J. Morel. High proportion ZnO/CuO nanocomposites:Synthesis, structural and optical properties, and their photocatalytic behavior. *Surfaces and Interfaces* **2019**, *17*, 100367, https://doi.org/10.1016/j.surfin.2019.100367.
3. K. Nakamura; K. Kanazawa; N. Kobayashi. Electrochemical photoluminescence modulation of functional materials and their electrochemical devices. *Journal of Photochemistry and Photobiology C: Photochemistry Reviews* **2022**, *50*, 100486, https://doi.org/10.1016/j.jphotochemrev.2022.100486.
4. M. Farhan; T.N. Reza; F.R. Badal; M.R. Islam; S.M. Muyeen; Z. Tasneem; M.M. Hasan; M.F.Ali; M.H. Ahamed; S.H. Abhi; M.M. Islam; S.K. Sarker; S.K. Das; P. Das. Towards next generation Internet of Energy system: Framework and trends. *Energy and AI* **2023**, *14*, 100306, https://doi.org/10.1016/j.egyai.2023.100306.
5. N. Goodarzi, Z. Ashrafi-Peyman, E. Khani, A.Z. Moshfegh. Recent Progress on Semiconductor Heterogeneous Photocatalysts in Clean Energy Production and Environmental Remediation. *Catalysts* **2023**, *13*, 1102, https://doi.org/10.3390/catal13071102.
6. Sebastian, M.T. CHAPTER NINE - CATION-DEFICIENT PEROVSKITES. In Dielectric Materials for Wireless Communication, Sebastian, M.T., Ed.; Elsevier: Amsterdam, **2008**; pp. 335-360, https://doi.org/10.1016/B978-0-08-045330-9.00009-1.
7. R. Sivasamy; P. Venugopal; R. Espinoza-González. Crystal structure, optical and magnetic properties of perovskite $Gd(Mn_0.7Ni_{0.3})O_3$ ceramic nanoparticles: An experimental and first-principles studies. *Ceramics International* **2019**, *45*, 20022-20027, https://doi.org/10.1016/j.ceramint.2019.06.262.
8. Nande, A.; Raut, S.; Dhoble, S.J. Chapter 9 - Perovskite solar cells. In Energy Materials, Dhoble, S.J., Kalyani, N.T., Vengadaesvaran, B., Kariem Arof, A., Eds.; Elsevier: **2021**; pp. 249-281, https://doi.org/10.1016/B978-0-12-823710-6.00002-9.
9. M. Zhang; W. Sun; H. Lv; Z.-H. Zhang. Syntheses and applications of perovskite-based photocatalysts in light-driven organic reactions. *Current Opinion in Green and Sustainable Chemistry* **2021**, *27*, 100390, https://doi.org/10.1016/j.cogsc.2020.100390.
10. R. Sivasamy; P. Venugopal; R. Espinoza-González. Structure, electronic structure, optical and magnetic studies of double perovskite Gd_2MnFeO_6 nanoparticles: First principle and experimental studies. *Materials Today Communications* **2020**, *25*, 101603, https://doi.org/10.1016/j.mtcomm.2020.101603.
11. M. Faizan; G. Murtaza; S.H. Khan; A. Khan; A. Mehmood; R. Khenata; S. Hussain. First- principles study of the double perovskites Sr_2XOsO_6 (X = Li, Na, Ca) for spintronics applications. *Bulletin of Materials Science* **2016**, *39*, 1419-1425, https://doi.org/10.1007/s12034-016-1288-6.
12. A. Masuno; H. Inoue; K. Yoshimoto; Y. Watanabe. Thermal and optical properties of La_2O_3-Nb_2O_5 high refractive index glasses. *Opt. Mater. Express* **2014**, *4*, 710-718, https://doi.org/10.1364/OME.4.000710.
13. I. Bibi; H. Maqbool; S. Iqbal; F. Majid; S. Kamal; N. Alwadai; M. Iqbal. $La_{1-x}Gd_xCr_{1-y}Ni_yO_3$ perovskite nanoparticles synthesis by micro-emulsion route: Dielectric, magnetic and photocatalytic properties evaluation. *Ceramics International* **2021**, *47*, 5822-5831, https://doi.org/10.1016/j.ceramint.2020.11.033.
14. H. Albalawi; G.M. Mustafa; S. Saba; N.A. Kattan; Q. Mahmood; H.H. Somaily; M. Morsi; S.Alharthi; M.A. Amin. Study of optical and thermoelectric properties of double perovskites Cs2KTlX6 (X = Cl, Br, I) for solar cell and energy harvesting. *Materials Today Communications* **2022**, *32*, 104083, https://doi.org/10.1016/j.mtcomm.2022.104083.
15. H. Hayun; R. Wolf; C. Barad; Y. Gelbstein. Thermal shock resistant solid oxide fuel cell ceramic composite electrolytes. *Journal of Alloys and Compounds* **2020**, *821*, 153490, https://doi.org/10.1016/j.jallcom.2019.153490.
16. J. Ahmed; N. Alhokbany; M. Ubaidullah; S. Mutehri; M.A.M. Khan; S.M. Alshehri. Synthesis of double perovskite La_2MnNiO_6 nanoparticles as highly efficient oxygen evolution electro- catalysts, *Ceramics International* **2020**, *46*, 20038-20044, https://doi.org/10.1016/j.ceramint.2020.05.075.
17. A. Taylor; H. Sinclair. On the determination of lattice parameters by the debye-scherrer method, *Proceedings of the Physical Society* **1945**, *57*, 126, https://doi.org/10.1088/0959-5309/57/2/306.
18. Ghodke, S.A.; Maheshwari, U.; Gupta, S.; Sonawane, S.H.; Bhanvase, B.A. Chapter 12 - Nanomaterials for adsorption of pollutants and heavy metals: Introduction, mechanism, and challenges. In Handbook of Nanomaterials for Wastewater Treatment, Bhanvase, B., Sonawane, S., Pawade, V., Pandit, A., Eds.;

Elsevier: **2021**; pp. 343-366, https://doi.org/10.1016/B978-0-12-821496-1.00032-5.
19. L.B. McCusker; R.B. Von Dreele; D.E. Cox; D. Louer, P. Scardi. Rietveld refinement guidelines. *Journal of Applied Crystallography* **1999**, *32*, 36-50, https://doi.org/10.1107/S0021889898009856.
20. L. Hu; J. Zhu; C. Duan; J. Zhu; J. Wang; K. Wang; Z. Gu; Z. Xi; J. Hao; Y. Chen; J. Ma; J.-X. Liu; C. Ma. Revealing the Pnma crystal structure and ion-transport mechanism of the Li3YCl6 solid electrolyte. *Cell Reports Physical Science* **2023**, *4*, 101428, https://doi.org/10.1016/j.xcrp.2023.101428.
21. U.V. Ghorpade; M.P. Suryawanshi; M.A. Green; T. Wu; X. Hao; K.M. Ryan. Emerging Chalcohalide Materials for Energy Applications. *Chemical Reviews* **2023**, *123*, 327-378, https://doi.org/10.1021/acs.chemrev.2c00422.
22. E.K. Albrecht; A.J. Karttunen. Investigation on the predictive power of tolerance factor τ forA-site double perovskite oxides. *Dalton Transactions*, **2023**, *52*, 12461-12469, https://doi.org/10.1039/D3DT01990J.
23. M. Amin; A.S. Alofi; T.M. Al-Daraghmeh; O. Zayed; M.m. Al-Anazy; A.I. Aljameel; M. Younas; R. Karmouch; Q. Mahmood; M. Adam. Role of 4d electrons in room temperature ferromagnetism, and thermoelectric properties of $Sr_2Cr_XO_6$ (X = Nb, Mo) for spintronic applications. *Materials Chemistry and Physics*, **2024**, *312*, 128643, https://doi.org/10.1016/j.matchemphys.2023.128643.
24. N. Ahn; K. Kwak; M.S. Jang; H. Yoon; B.Y. Lee; J.-K. Lee; P.V. Pikhitsa; J. Byun; M. Choi. Trapped charge-driven degradation of perovskite solar cells. *Nature Communications* **2016**, *7*, 13422, https://doi.org/10.1038/ncomms13422.
25. R. Yogamalar; R. Srinivasan; A. Vinu; K. Ariga; A.C. Bose. X-ray peak broadening analysisin ZnO nanoparticles. *Solid State Communications* **2009**, *149*, 1919-1923, https://doi.org/10.1016/j.ssc.2009.07.043.
26. R. Sivasamy; P. Venugopal; E. Mosquera. Synthesis of Gd_2O_3/CdO composite by sol-gel method: Structural, morphological, optical, electrochemical and magnetic studies. *Vacuum*, **2020**, *175*, 109255, https://doi.org/10.1016/j.vacuum.2020.109255.
27. S. Ramesh; J.V. Ramaclus; E. Mosquera; B.B. Das. Sol-gel synthesis, structural, optical and magnetic characterization of $Ag_{3(2+x)}Pr_xNb_{4-x}O_{11}+\delta$ ($0.0 \leq x \leq 1.0$) nanoparticles. *RSC Advances* **2016**, *6*, 6336-6341, https://doi.org/10.1039/C5RA24925B.
28. T. Frömling; Y. Liu; A.-P. Hoang; M. Gehringer; S. Steiner; M. Zhuk; J. Glaum; B.-X. Xu. Modulus spectroscopy for the detection of parallel electric responses in electroceramics. *Journal of Materiomics* **2022**, *8*, 556-569, https://doi.org/10.1016/j.jmat.2021.12.005.
29. Floudas, G. 2.32 - Dielectric Spectroscopy. In Polymer Science: A Comprehensive Reference, Matyjaszewski, K., Möller, M., Eds.; Elsevier: Amsterdam, **2012**; pp. 825-845, https://doi.org/10.1016/B978-0-444-53349-4.00057-1.
30. P. Satya Gopal Rao, R. Siripuram, S. Sripada. Impedance analysis of TeO_2-SeO_2-Li_2O nanoglass system. *Results in Physics*, **2019**, *13*, 102133, https://doi.org/10.1016/j.rinp.2019.02.069.
31. M.M. Abdullah. Consequences of frequency and temperature on the ac-conductivity in ε- GaSe semiconductor single crystal. *Results in Physics*, **2021**, *25*, 104220, https://doi.org/10.1016/j.rinp.2021.104220.
32. Pluta, T.; Skrzyński, G. Chapter Fifteen - Time-dependent DFT calculations of the dipole moment and polarizability for excited states. In Advances in Quantum Chemistry, Musial, M., Hoggan, P.E., Eds.; Academic Press: **2021**; Volume 83, pp. 305-327, https://doi.org/10.1016/bs.aiq.2021.05.005.
33. Kao, K.C. 2 - Electric Polarization and Relaxation. In Dielectric Phenomena in Solids, Kao, K.C., Ed.; Academic Press: San Diego, **2004**; pp. 41-114, http://dx.doi.org/10.1016/B978-012396561-5/50012-8.
34. Y.A. Genenko; J. Glaum; M.J. Hoffmann; K. Albe. Mechanisms of aging and fatigue in ferroelectrics. *Materials Science and Engineering: B* **2015**, *192*, 52-82, https://doi.org/10.1016/j.mseb.2014.10.003.
35. N.K. Elangovan; R. Kannadasan; B.B. Beenarani; M.H. Alsharif; M.-K. Kim; Z. Hasan Inamul. Recent developments in perovskite materials, fabrication techniques, band gap engineering, and the stability of perovskite solar cells. *Energy Reports* **2024**, *11*, 1171-1190, https://doi.org/10.1016/j.egyr.2023.12.068.
36. J. Naik; R.F. Bhajantri; S.G. Rathod; T. Sheela; V. Ravindrachary. Synthesis and characterization of multifunctional ZnBr2/PVA polymer dielectrics. *Journal of Advanced Dielectrics* **2016**, *06*, 1650028, https://doi:10.1142/S2010135X16500284.
37. Zhou, X.; Yu, D.; Barrera, O. Chapter Three - Mechanics constitutive models for viscoelastic solid materials: Development and a critical review. In Advances in Applied Mechanics, Bordas, S.P.A., Ed.; Elsevier: **2023**; Volume 56, pp. 189-321, http://dx.doi.org/10.1016/bs.aams.2022.09.003.
38. Q. Hu; J. Bian; Y. Zhuang; Z. Huang; G. Liu; V. Shur; Z. Xu; X. Wei. Debye-like relaxationbehavior and

electric field induced dipole re-orientation of the $0.6BaTiO_3$ −$0.4Bi(Mg_{1/2}Ti_{1/2})O_3$ Ceramic. *Ceramics International* **2017**, *44*, 922-930, https://doi.org/10.1016/j.ceramint.2017.10.024.

39. Hore, P.J. NMR Principles. In Encyclopedia of Spectroscopy and Spectrometry, 1st Editioin; Lindon, J.C., Tranter, G.E.; Holmes, J.L., Eds.; Academic Press: **1999**; pp. 1545-1553.
40. Xin, Q. 2 - Durability and reliability in diesel engine system design. In Diesel Engine System Design, Xin, Q., Ed.; Woodhead Publishing: **2013**; pp. 113-202, http://dx.doi.org/10.1533/9780857090836.1.113.
41. Varshneya, A.K.; Mauro, J.C. Chapter 15 - Dielectric properties. In Fundamentals of Inorganic Glasses (Third Edition), Varshneya, A.K., Mauro, J.C., Eds.; Elsevier: **2019**; pp. 425-442, https://doi.org/10.1016/B978-0-12-816225-5.00015-8.
42. German, R.M. Chapter Seven - Thermodynamic and Kinetic Treatments. In Sintering: from Empirical Observations to Scientific Principles, German, R.M., Ed.; Butterworth-Heinemann: Boston, **2014**; pp. 183-226, https://doi.org/10.1016/B978-0-12-401682-8.00007-0.
43. Biron, M. 7 - Advanced Environmental and Engineering Properties to Support Eco-Design for Plastics. In A Practical Guide to Plastics Sustainability, Biron, M., Ed.; William Andrew Publishing: **2020**; pp. 309-369, https://doi.org/10.1016/B978-0-12-821539-5.00007-0.
44. H.M. Chenari, M.M. Golzan, H. Sedghi, A. Hassanzadeh, M. Talebian. Frequency dependence of dielectric properties and electrical conductivity of Cu/nano-SnO2 thick film/Cu arrangement. *Current Applied Physics* **2011**, *11*, 1071-1076, https://doi.org/10.1016/j.cap.2011.01.038.